ACTA METALLURGICA SLOVACA
2024, VOL. 30, NO. 2, 72-76

RESEARCH PAPER

NOVEL INSIGHTS INTO PHASE FORMATION AND ELECTRICAL RESISTIVITY OF FeSe ALLOY PREPARED BY POWDER METALLURGY METHOD

Dea Nita Deslia Sari[1], Ryan Fitriandhani[2], Andika Widya Pramono[3], Agung Imaduddin[3], Sigit Dwi Yudanto[4]

[1]*Department of Physics, Universitas Sumatera Utara, Medan, Sumatera Utara, 20222, Indonesia*
[2]*Department of Mechanical Engineering, Institut Teknologi PLN, Jakarta Barat, 11750, Jakarta, Indonesia*
[3]*Research Center for Advanced Materials, National Research and Innovation Agency, Gedung 720, KST BJ Habibie, Serpong, Tangerang Selatan, Banten, 15314, Indonesia*
[4]*Research Center for Metallurgy, National Research and Innovation Agency, Gedung 720, KST BJ Habibie, Serpong, Tangerang Selatan, Banten, 15314, Indonesia*

*Corresponding author: sigi012@brin.go.id, tel.: +6281213024663

Received: 22.05.2024
Accepted: 23.05.2024

ABSTRACT

This study prepared the FeSe alloy using a powder metallurgy route. The Fe and Se powders were weighed at an atomic ratio of Fe:Se = 1.025:1 and milled for 5 hours. A simultaneous thermal analysis (STA) was performed to observe the behavior of the milled powder during thermal changes. After packing the milled powder in a stainless-steel tube, it was compacted. Investigation was performed to observe how the tetragonal FeSe phase forms at sintering temperatures of 718 K, 818 K, and 918 K. At a sintering temperature of 718 K, the tetragonal FeSe phase was formed, as determined by our quantitative analysis of XRD. The highest tetragonal FeSe phase fraction of 68.46 wt.% was obtained at a temperature of 918 K. The lattice constants of the tetragonal FeSe for the best sample were a = 0.3773 nm and c = 0.5520 nm. The resistivity test demonstrated that all samples have a conductor phenomenon exceeding 16 K, with a maximum Tc-onset value of 15.11 K.

Keywords: FeSe; powder metallurgy; tetragonal; lattice; resistivity

INTRODUCTION

Since the early 19th century, superconducting materials have improved significantly, with a focus on zero resistance at very low temperatures. Due to the low critical temperature of superconductors to date, researchers are emphasizing their efforts to develop superconducting materials near room temperature. The temperature where materials lose their resistance is known as the critical temperature. It is possible that superconducting materials could have critical temperatures close to room temperature, as reported in reports of high-temperature superconducting oxide-based materials [1], [2].
In addition to the ongoing efforts to raise the critical temperature of superconducting materials, there have been discoveries of several new materials that possess superconducting properties. The superconducting characteristics of FeSe-based materials were reported by Hsu and colleagues in 2008 [3]. The critical temperature (Tc) for the FeSe material is 8 K [3]. The Tc value of this FeSe-based material increases to 15 K when tellurium (Te) is doped at the Se site [4]. Sun, et al. reported that the critical temperature of $FeSe_{0.9}Te_{0.057}S_{0.043}$ has increased from 8.5 K to 10.43 K [5]. It is claimed that the critical temperature of FeSe-based materials is 30 K in the FeSe, even when substituted with potassium ($K_{0.8}Fe_2Se_2$) [6].
Li, et al. investigated the formation of FeSe-based superconducting materials through the solid-state reaction procedure [7]. The highest volume fraction and the Tc value of the tetragonal FeSe phase were reported by Li, et al. to be >75% and 10.1 K, respectively [7]. According to Zhang, et al., the optimal stoichiometric ratio and milling time for forming the tetragonal FeSe phase using the mechanical milling technique were Fe/Se=1.20/1 and 6 hours [8], [9].
The powder metallurgy process was used to form a FeSe alloy with a tetragonal crystal system, as discussed in this paper. The influence of sintering temperature variations on the formation of tetragonal FeSe phase and electrical resistivity has been extensively studied.

MATERIAL AND METHODS

Material Preparation

Synthesis of FeSe-based alloys was done using the powder metallurgy method. The first step was to weigh and mix commercial iron powder (Merck, 99%) and selenium powder (Merck, 99%) with an atomic ratio of Fe: Se = 1.025:1. The mixed powder was milled in a shaker mill for 5 hours at a ball-to-powder weight ratio (BPR) of 6:1. The selenium diffusion reaction was then

maintained during the sintering process by insulating the milled powder in a stainless-steel (SS) tube (melting point of the selenium = ~493 K) [10]. This technique was applied in our earlier research [11], [12]. The milled powder was sealed and compacted at 350 MPa in a stainless-steel tube, and then heated for 6 hours at different temperatures of 718 K, 818 K, and 918 K. Three samples were obtained from this heating process, and they were designated as samples A, B, and C, respectively. The heating was conducted in open air with a temperature rise rate of 5 K/min.

Material Characterization

Simultaneous thermal analysis (STA) tests were performed using the LINSEIS STA Platinum series instrument to investigate the thermal behavior of the milled powder. In the condition of nitrogen (N_2) gas, the STA test was conducted at a temperature increase rate of 10 K/min.
The formation of the phase was determined by using an XRD Panalytical X'Pert MPD with Cu-Kα radiation. The qualitative analysis of the XRD was completed using the Match! software (evaluation version) equipped with the Crystallography Open Database (COD) 2018. By fitting the diffraction pattern, the phase composition and lattice parameters can be calculated by using the Rietveld method [13]. The samples' fracture surface and elemental composition were examined using a JEOL JSM-6390LA scanning electron microscope (SEM) and energy dispersive spectroscopy (EDS). The cryogenic magnetometer was employed to measure the electrical resistance of the sintered sample using a Four Point Probe (FPP) method.

RESULTS AND DISCUSSION

XRD Analysis

Fig. 1 shows the STA curve of the Fe and Se powder that has been milled. Endothermic peaks are present on two of the three primary peaks on the STA curve, while exothermic peaks are present. An endothermic peak 1 at 495 K represents the melting of selenium [7]. A heat absorption reaction takes place at 568 K. According to Li, et al., heating at a temperature over the melting point of selenium led to the formation of the Fe_3Se_4 and Fe_7Se_8 phases [7]. Due to the mobility of molten selenium, the reactions between Fe and Se are accelerated due to the rapid diffusion of atoms and the increased contact surface of reactants. The formation of Fe_3Se_4 and Fe_7Se_8 phases takes place at a temperature of 603 K [7]. At temperatures below 603 K, the Fe_7Se_8 phase is transformed into the tetragonal FeSe or β-FeSe phase. Peak 3 at 610 K represents the heat released during the phase change process. The β-FeSe continues to form when the temperature reaches 636 K [7].

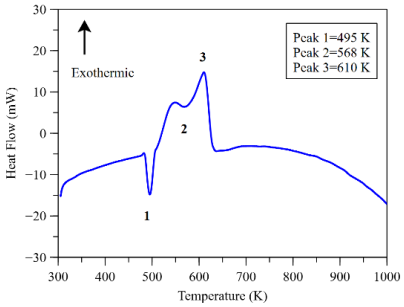

Fig. 1 The STA curve of the milled powder (as-milled)

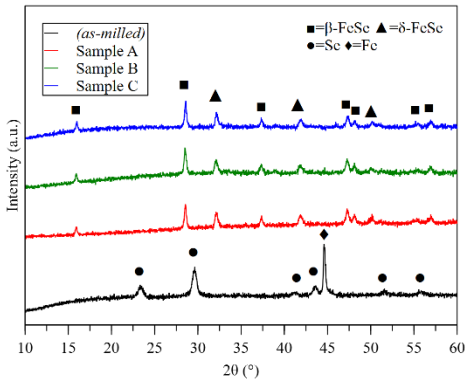

Fig. 2 Powder XRD of FeSe-based samples with various temperature sintering compared to as-milled powder

The diffraction patterns of the FeSe-based samples sintered at 718 K, 818 K, and 918 K in comparison to the as-milled powder are shown in **Fig. 2**. The peak in the as-milled powder is related to the peak of Fe and Se phases, as indicated by the diffraction pattern. The Fe peaks correspond to COD database #901-6481, while the Se peaks correspond to COD database #900-8580. By comparing the sample. A to the as-milled powder, it was evident that a new phase had formed because phase peaks were not present in the constituent elements. The heating process resulted in forming a new peak known as the FeSe phase. The FeSe phase formed in all samples (Sample A, sample B and sample C) has two different crystal systems: the tetragonal crystal system (β-FeSe phase) and the hexagonal crystal system (δ-FeSe phase). The β-FeSe phase was found at 2θ = 15.98°, 28.56°, 37.33°, 47.31°, and 48.10° in accordance with the COD #432-9646. While the δ-FeSe phase was found at 2θ = 32.07°, 41.85°, and 50.17° in accordance with the COD # 901-5077. Increased sintering temperature caused a decrease in the peak intensity of the β-FeSe phase at 2θ = 41.85°. The FeSe-based alloys were successfully synthesized without needing a vacuum technique or a flowing inert gas, and the heating procedure does not result in any oxidation.
By analyzing the diffraction pattern, the phase mass fraction can be calculated with the Rietveld method. The plot of calculation and observation of diffraction patterns for FeSe-based samples is depicted in **Fig. 3**. The calculated β-FeSe phase lattice constants value for the sample C were lattice a = 0.3773 nm, and lattice c = 0.5520 nm. **Table 1** contains the quantitative results for the XRD test. As the temperature increased, the β-FeSe phase mass fraction rose from 62.01% to 68.46%. Comparing this result to the previous research by Li, et al., we see an improvement [7]. According to Li, et al., the volume fraction of the β-FeSe phase was around 30% upon heating to 723 K [7].
The crystallite size is calculated using the results of the diffraction pattern fitting shown in **Fig. 3**. The Monshi-Scherrer equation was used to estimate the crystallite size in the FeSe-based samples. Following the Scherrer equation, the Monshi-Scherrer equation is shown in Equation (1) [14], [15].

$$\ln \beta = ln\frac{K\lambda}{D} + ln\frac{1}{cos\theta} \quad (1.)$$

where β is the FWHM value of the phase peaks (radians), K is the Scherrer constant (0.94), λ is the wavelength of the radiation source beam (Cu Kα = 0.15406 nm), D is the crystallite size (nm) and θ is the phase peak angle (°). From Equation (1), the curve ln (1/cos θ) vs ln β for each sample is created as shown in **Fig.**

4. The estimated crystallite size of the FeSe-based samples formulated as follows Equation (2),

$$e^{ln\frac{K\lambda}{D}} = \frac{K\lambda}{D} \quad (2.)$$

The results of calculating the crystallite size for each sample using the Monshi-Scherrer equation are displayed in **Table 1**.

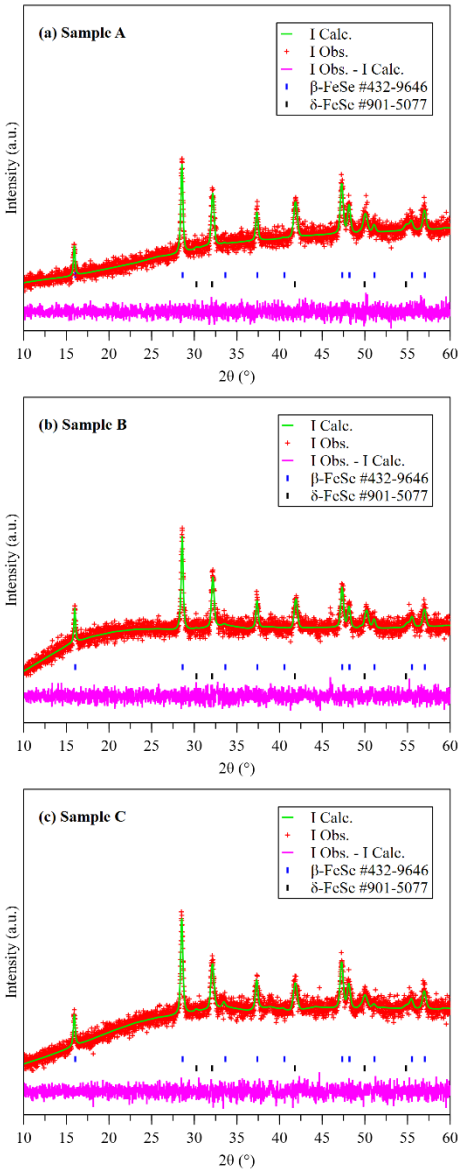

Fig. 3 The plot of calculation and observation diffraction pattern of the FeSe-based samples. (a) Sample A, (b) Sample B, and (c) Sample C

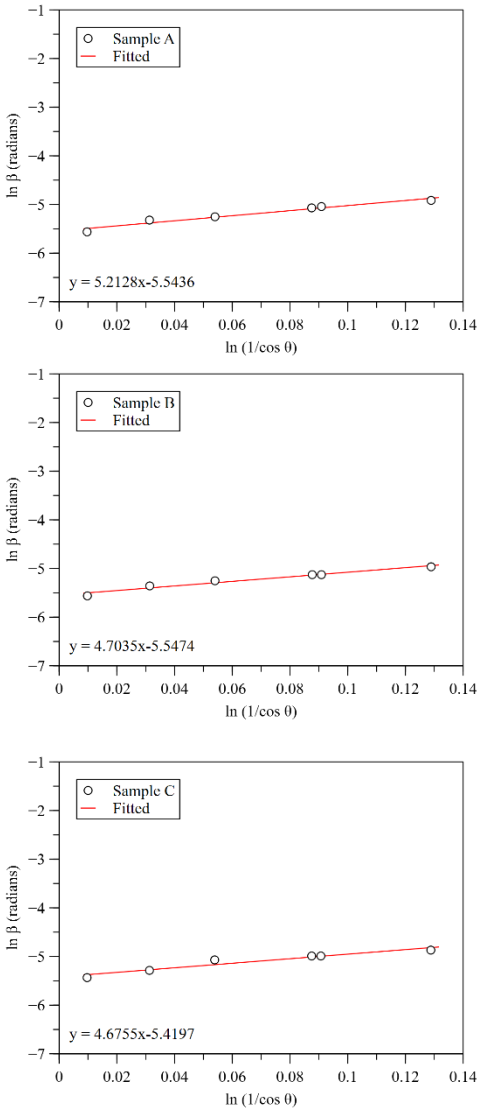

Fig. 4 Linear fit plot of ln (1/cos θ) vs ln β of the samples A, B, C

Table 1 Phase composition, lattice constants, and crystallite size of the FeSe-based samples

Source	Sample A	Sample B	Sample C
β-FeSe (wt.%)	62.01	64.75	68.46
δ-FeSe (wt.%)	37.99	35.25	31.54
Lattice ***a***-axis (nm)	0.3772	0.3775	0.3773
Lattice ***c***-axis (nm)	0.5522	0.5516	0.5520
GoF	1.185	1.159	1.158
Rp (%)	4.00	3.79	3.63
wRp (%)	5.04	4.76	4.62
D (nm)	37.01	37.16	32.70

SEM-EDS Analysis

Fig. 5 shows a scanning electron micrograph image of the FeSe-based samples with different sintering temperatures. The particles in sample A were observed to be small, uniform, and dense. As the temperature of sintering raises, some particles get bigger and have a more uniform grain shape. An energy dispersive spectroscopy (EDS) test was carried out to determine the elemental composition of the sample. The elemental composition test sample was selected for the area 002 of sample C. The EDS curve for area 002 of sample C is shown in **Fig. 6**, and **Table 2** shows the components detected there. The area 002 of sample C has a ratio of Fe: Se of 41.32: 58.68. According to the FeSe phase diagram, a selenium composition of 57.6–58.0 wt% results in the formation of the β-FeSe phase. With a selenium content of 58.1-66.0 wt.%, the δ-FeSe phase is formed. This agrees with **Fig. 2**, which shows the formation of the β-FeSe and the δ-FeSe. The non-superconducting δ-FeSe phase decreased due to the higher Fe content in the FeSe phase, according to Zhang, et al [8]. Therefore, controlling the stoichiometric ratio is important for forming the β-FeSe phase.

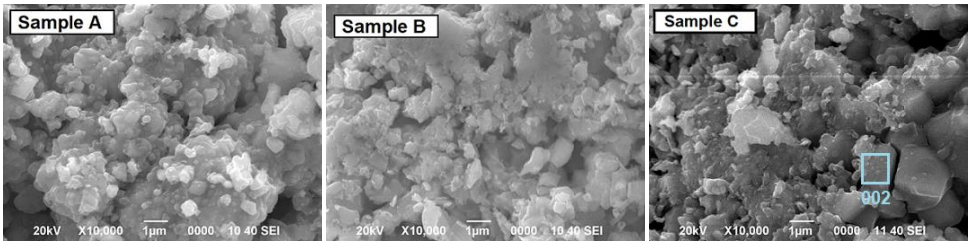

Fig. 5 The surface image of the FeSe-based samples with three sintering temperatures

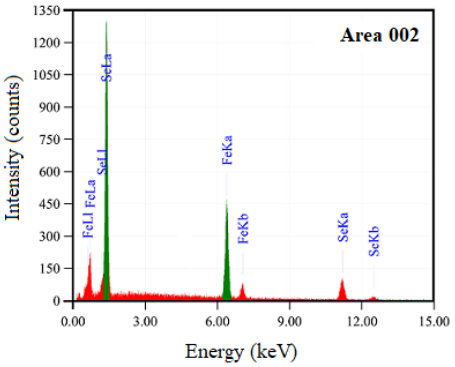

Fig. 6 The EDS curve of the sample C in area (002)

Table 2 Elemental composition of the sample C (area 002)

Element	at.%	wt.%
Fe	49.89	41.32
Se	50.11	58.68

Resistivity Measurement

To measure the electrical properties of the synthesized samples, a cryogenic magnetometer was used without any magnetic field. **Fig. 7** shows the relationship between temperature and resistivity. The resistivity value of the sintered sample, measured at 265 K, shows a decrease in resistivity value with decreasing temperature. The resistivity value of sample C drastically decreased at 15.11 K. When the resistivity temperature decreases significantly, it is referred to as the critical onset temperature (Tc-onset). This Tc-onset value is higher than in earlier research, which could be attributed to the compaction pressure [16]. The absence of superconducting properties in the three samples may be caused by a high concentration of the non-superconducting FeSe phase (hexagonal phase or δ-FeSe).

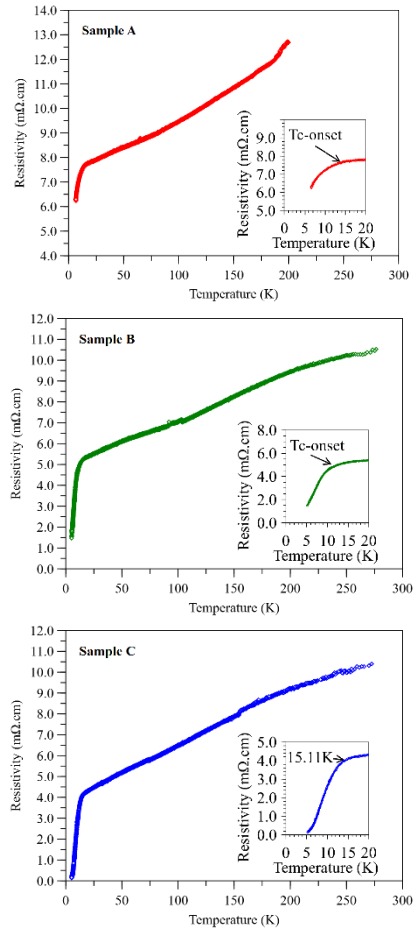

Fig. 7 Temperature dependence of resistivity for FeSe-based samples. The inset image shows Tc-onset value

CONCLUSION

The powder metallurgy method has been successfully used to synthesize FeSe alloys. FeSe alloy features tetragonal (β-FeSe) and hexagonal (δ-FeSe) crystal system. According to XRD analysis, the mass fraction of the β-FeSe superconducting phase increased as the sintering temperature was raised. The highest phase fraction of the β-FeSe phase generated in the sample when sintered at 918 K was 68 wt.%. According to resistivity measurements, the Tc-onset value of the β-FeSe phase with lattice constants a = 0.3773 nm and c = 0.5520 nm is 15.11 K.

Acknowledgements: The authors thank the Research Center for Metallurgy—National Research and Innovation Agency (BRIN) for providing the funding and research facilities.

REFERENCES

1. H. Maeda, Y. Tanaka, M. Fukutomi, T. Asano: Japanese Journal of Applied Physics, 27(2), 1988, L209–L210. https://doi.org/10.1143/JJAP.27.L209.
2. A. Schilling, M. Cantoni, J. D. Guo, H. R. Ott: Nature, 363, 1993, 56–58. https://doi.org/10.1038/363056a0.
3. F. C. Hsu, J. Y. Luo, K. W. Yeh, T. K. Chen, T. W. Huang, P. M. Wu, Y. C. Lee, Y. L. Huang, Y. Y. Chu, D. C. Yan, M. K. Wu: Proceedings of the National Academy of Sciences of the United States of America, 105(38), 2008, 14262–14264. https://doi.org/10.1073/pnas.0807325105.
4. Y. Mizuguchi, F. T. Omioka, S. T. Suda: Journal of the Physical Society of Japan, 78(7), 2009, 1–5. https://doi.org/10.1143/JPSJ.78.074712.
5. F. Sun, Z. Guo, H. Zhang, W. Yuan, Journal of Alloys and Compounds, 700, 2017, 43–48. https://doi.org/10.1016/j.jallcom.2017.01.064.
6. J. Guo, S. Jin, G. Wang, S. Wang, K. Zhu, T. Zhou, M. He, X. Chen: Physical Review B, 82(18), 2010, 180520. https://doi.org/10.1103/PhysRevB.82.180520.
7. X. Li, Z. Ma, Y. Liu, M. Dong, L. Yu: IEEE Transactions on Applied Superconductivity, 23(2), 2013, 7000405. https://doi.org/10.1109/TASC.2013.2246159.
8. S. Zhang, J. Liu, J. Feng, C. Li, X. Ma: Journal of Materiomics, 1, 2015, 118–123. https://doi.org/10.1016/j.jmat.2015.04.004.
9. S. Zhang, X. Ma, J. Liu, J. Feng, C. Li, P. Zhang: Materials Science Forum, 848, 2016, 657–663. https://doi.org/10.4028/www.scientific.net/MSF.848.657.
10. Okamoto, Journal of Phase Equilibria, 12(3), 1991, 368–372. https://doi.org/10.1007/BF02649932.
11. S. D. Yudanto, R. Fitriandhani, A. W. Pramono, A. Imaduddin, B. Kurniawan: Key Engineering Materials, 855, 2020, 96–101. https://doi.org/10.4028/www.scientific.net/KEM.855.96.
12. M. Y. Hasbi, S. A. Chandra, A. Fitriani: Science of Sintering, 55, 2023, 81–88. https://doi.org/10.2298/SOS2301081Y.
13. A. C. Larson, R. B. Von Dreele, Los Alamos National Laboratory Report, pp. 1–224, 2004.
14. A. Monshi, M. R. Foroughi, M. R. Monshi: World Journal of Nano Science and Engineering, 02(03), 2012, 154–160. https://doi.org/10.4236/wjnse.2012.23020.
15. S. D. Yudanto, S. A. Chandra, R. Roberto, D. P. Utama, V. O. Herlina, Lusiana: Journal of Ceramic Processing Research, 23(3), 2022, 287–291. https://doi.org/10.36410/jcpr.2022.23.3.287.
16. Y. Mizuguchi, F. Tomioka, S. Tsuda, T. Yamaguchi, Y. Takano, Applied Physics Letters, 93, 2008, 152505. https://doi.org/10.1063/1.3000616.